Journal of Energy Storage 143 (2026) 119608

Contents lists available at ScienceDirect

Journal of Energy Storage

journal homepage: www.elsevier.com/locate/est

Research papers

Revealing the reversible hydrogen storage potential of light transition-metal decorated organic C_5N monolayers

Pawitnus Kerdsombut [a], Pathipat Latthiwan [a], Niphat Thatsami [a], Pakpoom Reunchan [b], Adisak Boonchun [b], Tanveer Hussain [c,*], Supree Pinitsoontorn [a,d], Thanayut Kaewmaraya [a,d,**]

[a] Computational Advanced Materials Physics Group (CAMP), Department of physics, Khon Kaen University, Khon Kaen, 40002, Thailand
[b] Department of Physics, Faculty of Science, Kasetsart University, Bangkok, 10900, Thailand
[c] School of Science and Technology, University of New England, Armidale, New South Wales, 2351, Australia
[d] Institute of Nanomaterials Research and Innovation for Energy (IN-RIE), NANOTEC-KKU RNN on Nanomaterials Research and Innovation for Energy, Khon Kaen University, Khon Kaen, 40002, Thailand

ARTICLE INFO

Keywords:
Hydrogen storage
C_5N
Thermodynamic analysis
Kubas-type interaction

ABSTRACT

Fuel-cell vehicles (FCVs) offer compelling advantages for sustainable transportation, including rapid refueling, extended driving range, and zero CO_2 emissions. However, the current reliance on highly pressurized hydrogen (H_2) tanks presents significant challenges in terms of safety, operational pressure, and storage capacity. Moving beyond conventional compressed gas storage, this study explores a solid-state H_2 storage paradigm based on light, nanoporous organic penta-carbon nitride (C_5N) decorated with light transition metals (TMs). Using density functional theory (DFT), thermodynamic analysis, and *ab-initio* molecular dynamics (AIMD), we show that selected TMs, Sc, Ti, and V, can be energetically anchored onto C_5N without clustering, owing to the synergy between their strong binding energies and high diffusion barriers. The TM-decorated C_5N exhibit reversible H_2 adsorption *via* peculiar Kubas-type interactions, achieving high theoretical gravimetric densities of 5.81, 5.73, and 5.65 wt% for Sc, Ti, and V@C_5N, respectively. These numbers surpass the U.S. Department of Energy (DOE) target of 5.50 wt%. Notably, Sc@C_5N and V@C_5N also demonstrate the ability to store H_2 under practical ranges of temperatures and pressures, with reversible adsorption at 5.0 bar and desorption at practically low temperatures (below 85.0 °C). Our findings conclusively propose TM-decorated C_5N as highly promising candidates for H_2 storage in FCVs.

1. Introduction

Efficient hydrogen storage (H_2-storage) plays a central role in hydrogen economy, enabling applications such as fuel cell vehicles (FCVs), grid-scale energy storage, ammonia and methanol production, steelmaking, and residential heating [1–6]. In particular, the current storage technology for FCVs relies on carbon fiber composite tanks, which are lightweight, extremely strong, and capable of withstanding both internal and external pressures. Although they can store up to 5.5 wt% of H_2 according to the target value set by the U.S. Department of Energy (DOE), their high cost, extreme compression (up to 700.0 bar) for reducing the storage size, and safety are the major hindrances [7–10]. Beyond the conventional methods, H_2-storage based on nanoporous solid materials with high surface area has emerged as a promising route because of the ultra-high capacity with reduced storage size [11,12]. Metal hydrides such as MgH_2 [13,14], $LiBH_4$ [15], and $NaBH_4$ [16] exemplify the exceptional storage capacity (5.5 to 10.0 wt%) and safety. Despite, these materials critically suffer from the sluggish reversible reaction kinetics during the adsorption-desorption cycles of H_2 molecules. In this regard, high temperatures or catalysts can be employed to accelerate chemical kinetics.

The slow reaction kinetics is fundamentally attributed to the exaggerated chemical bonds formed between H_2 molecules and the storage materials (*i.e.*, chemisorption). The chemisorption gives rise to the high storage capacity because of the enhanced number of H_2 molecules, but it raises the desorption temperatures which retard the chemical kinetics.

* Corresponding author.
** Correspondence to: T. Kaewmaraya, Computational Advanced Materials Physics Group (CAMP), Department of physics, Khon Kaen University, Khon Kaen, 40002, Thailand.
E-mail addresses: tanveer.hussain@une.edu.au (T. Hussain), thakaew@kku.ac.th (T. Kaewmaraya).

https://doi.org/10.1016/j.est.2025.119608
Received 29 June 2025; Received in revised form 5 November 2025; Accepted 19 November 2025
Available online 27 November 2025

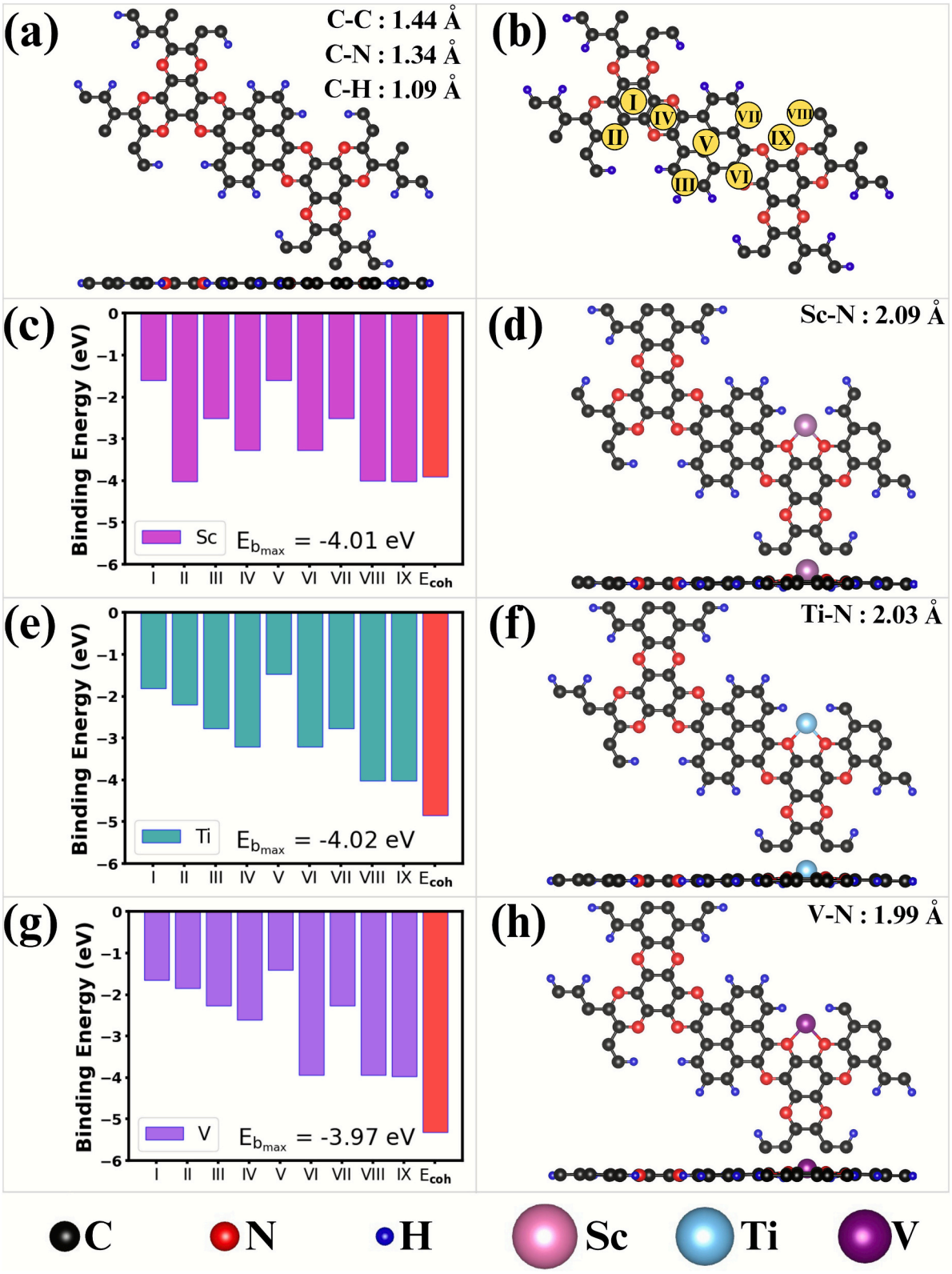

Fig. 1. (a) Optimized atomic structure of pristine C_5N, (b) possible adsorption sites of TMs on C_5N, and (c-h) binding energies of the TMs on various adsorption sites and the corresponding structures with the strongest binding energies.

This aspect can be resolved by using materials offering physisorption *via* weak van der Waals (vdW) interaction to capture H_2 molecules. The physisorption enables rapid adsorption and desorption, ideal for efficient cycling applications. Metal organic frameworks (MOFs) [17], covalent organic frameworks (COFs) [18], graphene [19], and carbon nanotubes [20,21] are notable examples of capturing H_2 molecules by predominantly weak vdW forces, offering the storage capacity (2.5 to 7.5 wt%). Nevertheless, the physisorption usually offers a lower storage capacity than chemisorption. Ideal storage materials should possess low atomic weights to be lightweights and store H_2 with moderate binding

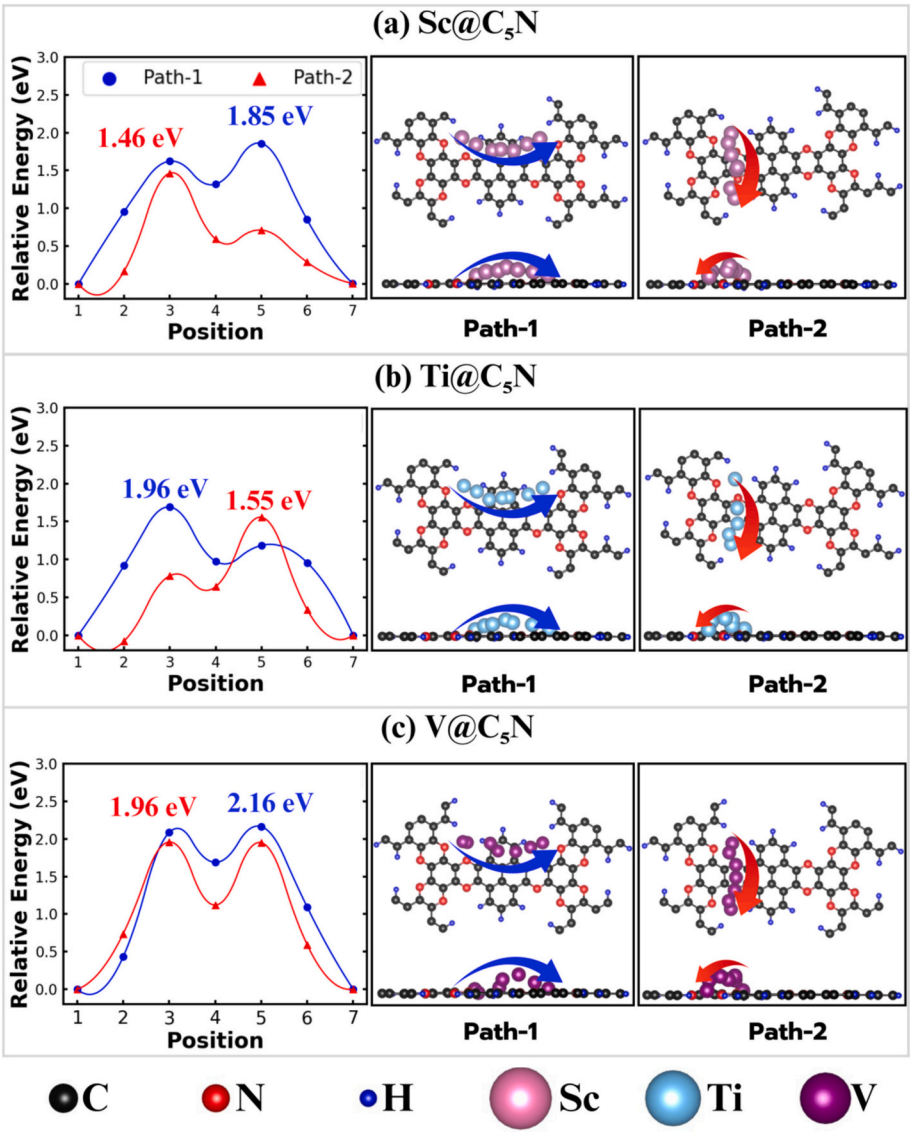

Fig. 2. Diffusion barriers of the metal atoms moving from the most stable position to the neighboring equivalent position along path-1 and path-2 for (a) Sc@C_5N, (b) Ti@C_5N, and (c) V@C_5N.

energies between weak vdW physisorption and strong chemisorption. Hence, searching for the appropriate materials fulfilling all these requirements is the critical challenge.

As described, the promising storage materials should be lightweight, high surface area, and have appropriate binding energies. In this regard, carbon nanomaterials have emerged as the intuitive candidates [15,16]. However, intrinsic C—C bonds show weak binding energies because of their lower affinity toward H_2 molecules. Surface modification, such as doping, defects, and heterostructure is required to magnify H_2 bindings [22–24]. Despite the satisfactory storage capacity of around 6.0 wt% achieved, some transitional metals decorated on carbon nanomaterials are problematic with surface clustering [22–24]. Moreover, the effective storage under ambient conditions remains elusive. These limitations have further driven the search for alternative light materials. Generic two-dimensional (2D) carbon-nitrides (C_xN_y) have emerged as candidates operating at standard pressures and temperatures mainly because of their lightweight, ultra-high surface area, and freedom to tune properties upon varying the x/y ratio [19,20]. In particular, the C—N bonds are more affinitive to the functionalized surface metal dopants, providing more stable metal decoration without aggregation [25,26]. For instance, Li@g-C_2N has demonstrated a high theoretical H_2 storage capacity of 13.00 wt%, with adsorption energies ranging from −0.12 to −0.23 eV/H_2 [27]. Furthermore, Al@g-CN showed significant potential, achieving a storage capacity of 6.15 wt% with adsorption energies between −0.11 and − 0.31 eV/H_2 [28]. Mg@g-C_3N_4 offers a storage capacity of 7.96 wt% and adsorption energies ranging from −0.10 to −0.25 eV/H_2 [29]. Mg + Li@g-C_3N_4 monolayer exhibits a high storage capacity of 10.01 wt% with adsorption energies between −0.10 and − 0.23 eV/H_2 [30]. Li@g-C_6N_6 and Li@g-$C_{10}N_3$ have achieved storage capacities of 5.88 and 8.00 wt% under moderate pressure, respectively [31]. However, non-transition metal decoration (*e.g.*, Li and Na) has some limitations in aggregation and instability due to the low diffusion barriers [32].

Beyond, surface decoration by transition metals (TMs) becomes a promising alternative because of the enhanced structural stability originating from the immense interaction of unpaired electron in C—N bonds with the unfilled *d*-orbitals of TMs. Consequently, TMs dopants possess feasible doping/synthesis techniques as endorsed by the success of single-atom catalysts (SACs) or dual-atom catalysts (DACs) [33,34]. The partially filled *d*-orbitals of the anchored TMs can effectively modulate the H_2 binding to be at the appropriate range between the chemisorption and physisorption, which is typically defined as Kubas-

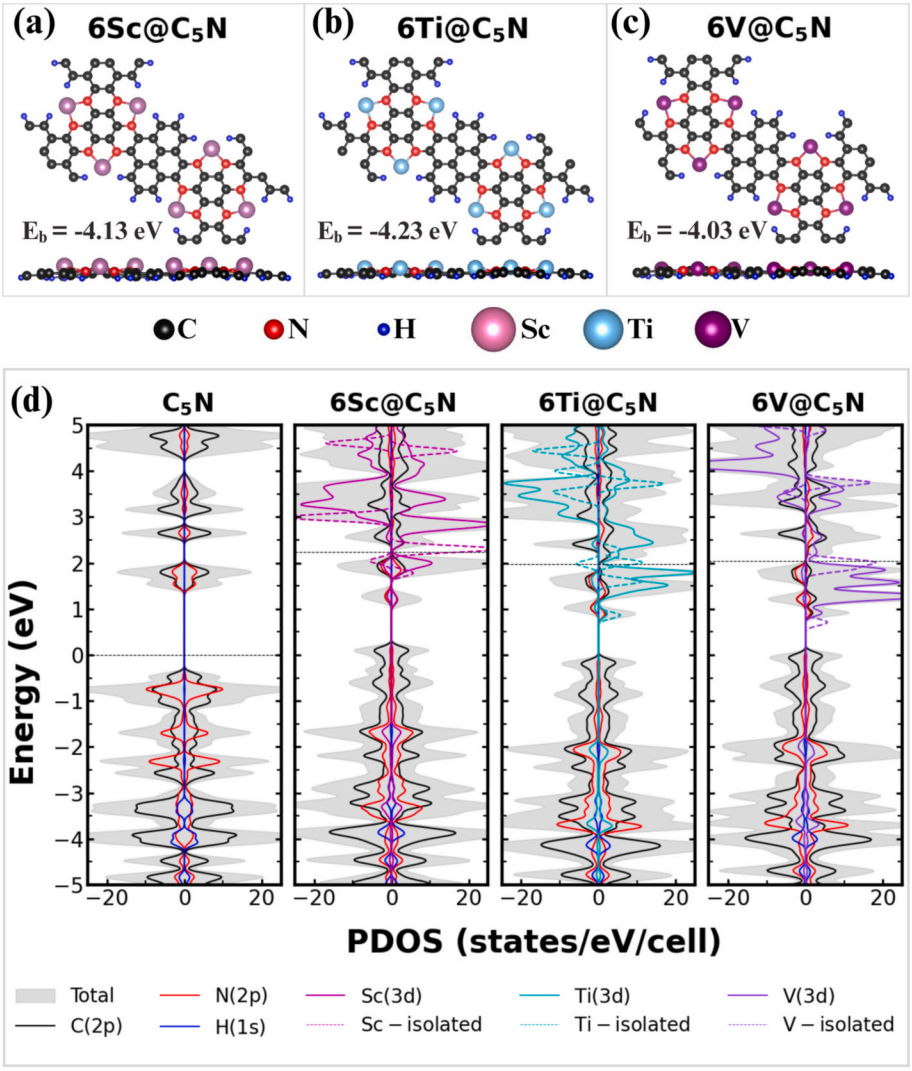

Fig. 3. Top and side views of the optimized atomic structures of (a) 6Sc@C_5N, (b) 6Ti@C_5N, and 6V@C_5N. (c) Projected density of states (PDOS) of pristine and 6TM@C_5N. The Fermi level is shown by the black dotted line.

type interaction [35,36]. This peculiar type of chemical interaction relies on the energetic electron donation from the σ bonding orbital of the H_2 molecule to the empty *d*-orbitals of the TMs. Simultaneously, an electron from the metal's *d*-orbital back-donates to the σ^* anti-bonding orbital of H_2. As a result, H—H bonds of the adsorbed H_2 molecules are destabilized and elongated, but they remain undissociatively bound in the molecular form with the appropriate binding energies for adsorption/desorption reversibility [37]. The binding energy ranged from 0.1 to 0.6 eV/H_2 is ideal for FCVs requiring reversible adsorption/desorption cycles at moderate temperatures and pressures [10]. According to these reasons, various TMs-decorated C_xN_y were demonstrated as promising H_2-stoage avenues. For example, Ti@C_2N offers the H_2-storage capacity of 6.8 wt%, with adsorption energies falling in the ideal range of −0.20 to −0.40 eV/H_2 [38]. TMs-decorated g-C_3N_4 could adsorb up to four H_2 molecules with adsorption energies of −0.30 to −0.60 eV/H_2, making them ideal for practical applications [39].

Recently, an organic 2D fused aromatic network (FAN) structure with a C_5N basal plane stoichiometry was successfully synthesized, making it distinctive from most inorganic C_xN_y [40]. The study demonstrates the material's exceptional electronic properties, including high charge carrier mobilities for both electrons (996 $cm^2/V{\cdot}s$) and holes (501 $cm^2/V{\cdot}s$), exceeding those of most undoped organic semiconductors. It also exhibits excellent thermal and chemical stability against oxidation. The C_5N monolayer is characterized as a direct bandgap semiconductor with an energy gap of 2.63 eV, showing strong absorption in the visible light spectrum suitable for photocatalytic water-splitting applications [41]. Moreover, the material possesses remarkable mechanical flexibility, with a tensile strength exceeding 10 GPa [41]. Notably, C_5N exhibits a moderate lattice thermal conductivity of approximately 9.5 $W{\cdot}m^{-1}\ K^{-1}$ at ambient temperature [41]. This balance between electrical and thermal transport is particularly advantageous for efficient Joule heating, enabling controlled release of adsorbed H_2 molecules. Inspired by the 2D nature with high surface area, high electrical conductivity, moderate thermal conductivity, significant mechanical flexibility, and thermal and chemical stabilities, organic C_5N is hypothesized to be a promising H_2 storage medium superior to the known inorganic C_xN_y.

Herein, we employ theoretical approaches including density functional theory (DFT), *ab-initio* molecular dynamics, and thermodynamics to unravel H_2 storage capacities of C_5N functionalized with TMs including Sc, Ti, and V. Our findings show that TMs-decorate C_5N are feasible H_2 storage materials because they offer the high volumetric densities of over 5.50 wt% at practical ranges of temperatures and pressures, fulfilling U.S. Department of Energy (DOE) 2025 requirement.

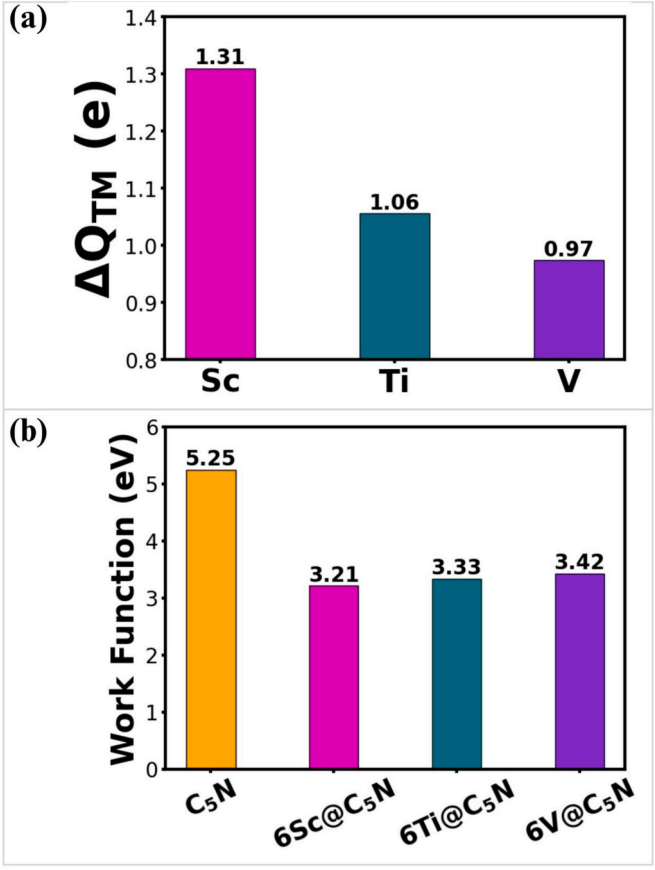

Fig. 4. (a) Bader charge analysis of charge transfer between TMs and C_5N and (b) Work functions of 6TM@C_5N.

2. Computational and modeling details

Theoretical calculations were performed using Vienna *Ab-initio* Simulation Package (VASP) within the framework of density functional theory (DFT). The exchange-correlation energy was approximated by the generalized gradient approximation of Perdew-Burke-Ernzerhof (GGA-PBE) approach [42]. The crystal structure of C_5N was modelled according to the experimental data, which consists of 90 atoms in a unit cell as shown in Fig. 1(a). The vacuum of 20.0 Å was added in the vertical direction to ensure the monolayer character. The cut-off energy of the plane wave basis of 500 eV was used, and the Brillouin zone integration was sampled by a Monkhorst-Pack grid of 3 × 3 × 1 for optimizing the atomic structures and a denser 6 × 6 × 1 for calculating the electronic density of states (DOS). The structural optimization was achieved when forces acting on all atoms became less than 50 meV/Å. The stopping-criterion for the electronic self-consistency loop was set to 10^{-6} eV.

The binding energy (E_b) of TMs-decorated C_5N was determined as the following equation:

$$E_b = (E_{m:TM@C_5N} - E_{C_5N} - mE_{TM})/m \quad (1)$$

where m refers to the number of TMs atoms adsorbed. Additionally, $E_{m:TM@C_5N}$,E_{C_5N}, and E_{TM} represent the total energy of TMs-decorated C_5N, bare C_5N monolayer, and isolated TMs atom, respectively. Meanwhile, the average adsorption energy (E_{ads}) for nH_2 molecules on TMs-decorated C_5N monolayer in the unit of eV/H_2 was determined as the following equation:

$$E_{ads} = (E_{m:TM@C_5N-nH_2} - E_{m:TM@C_5N} - nE_{H_2})/n \quad (2)$$

where $E_{m:TM@C_5N-nH_2}$, $E_{m:TM@C_5N}$, and E_{H_2} are the total energy of TMs-decorated C_5N monolayer adsorbed with nH_2 molecules, bare $E_{m:TM@C_5N}$ and isolated H_2 molecule, respectively. And n is the number of adsorbed H_2 molecules on TM-decorated C_5N monolayer. Here, the cut-off adsorption energy for further calculating the storage capacity is defined as −0.15 eV/H_2. In addition, Grimme method (DFT—D3) [43,44], was used throughout the computation to treat van der Waals (vdW) interactions predominantly existing between H_2 molecules and C_5N.

Subsequently, the gravimetric storage capacity was calculated as the following equation

$$\text{wt } (H_2)\% = nM_{H_2}/(nM_{H_2+}M_{mTM@C_5N}) \times 100 \quad (3)$$

where M_{H_2} and M_{C_5N} are the molecular masses of the isolated H_2 molecule and TM-decorated C_5N monolayer, respectively. Furthermore, the volumetric capacity was calculated by the following equation

$$V_{H_2} = (\text{mass of } nH_2 \text{ per unit cell})/(\text{volume of unit cell}). \quad (4)$$

The thermodynamic analysis was employed to calculate the adsorption-desorption characteristics at practical working conditions. The effective number of stored H_2 molecules (N_{eff}) adsorbed in the host material as a function of temperature (T) and pressure (P), which can be calculated by

$$N_{eff}(T,P) = [(Z-1)/Z]N_0 \quad (5)$$

where N_0 represents the number of H_2 molecules adsorbed on the host medium as obtained at 0.0 K (*i.e.*, Eq. 2), and Z defines the grand canonical partition function as the following equation

$$Z(E_{ads},T,P) = 1 + \sum_{i=1}^{n} e^{-\left(E^i_{ads}-\mu_{H_2}\right)/k_BT} \quad (6)$$

where E^i_{ads} is the average adsorption energy of the iH_2 molecule adsorbed, and the summation index i are 6, 12, 24, and 36. Note that the index i is the multiplication of 6 because there are 6 transition metal atoms (TMs) decorated on C_5N. Each TM atom successively adsorbs 1, 2, 4, and 6 H_2 molecules. Moreover, the parameter n defines the maximum number of H_2 molecules adsorbed on TMs-decorated C_5N, and it was determined according to the cut-off E_{ads} of −0.15 eV/H_2. Meanwhile, μ_{H_2} is and chemical potential of the gas phase of the H_2 molecule. In particular, μ_{H_2}, which is a function of P and T, is defined as

$$\mu_{H_2}(P,T) = \Delta H(T,P_0) - T\Delta S(T,P_0) + k_BT\ln\left(\frac{P}{P_0}\right) \quad (7)$$

where ΔH represents the enthalpy change accounting for translational, rotational, vibrational contributions of a H_2 molecule, ΔS is the entropy change, P is the pressure, and P_0 is the atmospheric pressure (1.01×10^5 Pa). The values of ΔH and TΔS are obtained from the experimental database and are provided in Table S1 of the Supplementary Information [45].

3. Results and discussion

3.1. Structural optimization and TMs-decorated C_5N

The optimized lattice parameter of the pristine C_5N monolayer is calculated to be 20.92 Å, consistent with previous reports [41]. The calculated bond lengths of C—C, C—N, and C—H are 1.44, 1.34, and 1.09 Å, respectively, as illustrated in Fig. 1(a). C_5N monolayer offers nine inequivalent adsorption sites for a H_2 molecule, denoted as sites I-IX, as shown in Fig. 1(b). These include site I (on the carbon ring), site II (above a nitrogen atom), site III (above a carbon atom), and site IV (on a carbon–nitrogen ring). Sites V, VI, and VII are located above the C—C, C—N, and C—H bonds, respectively. Site VIII lies directly above a H atom of C_5N, while site IX corresponds to a hollow region adjacent to N

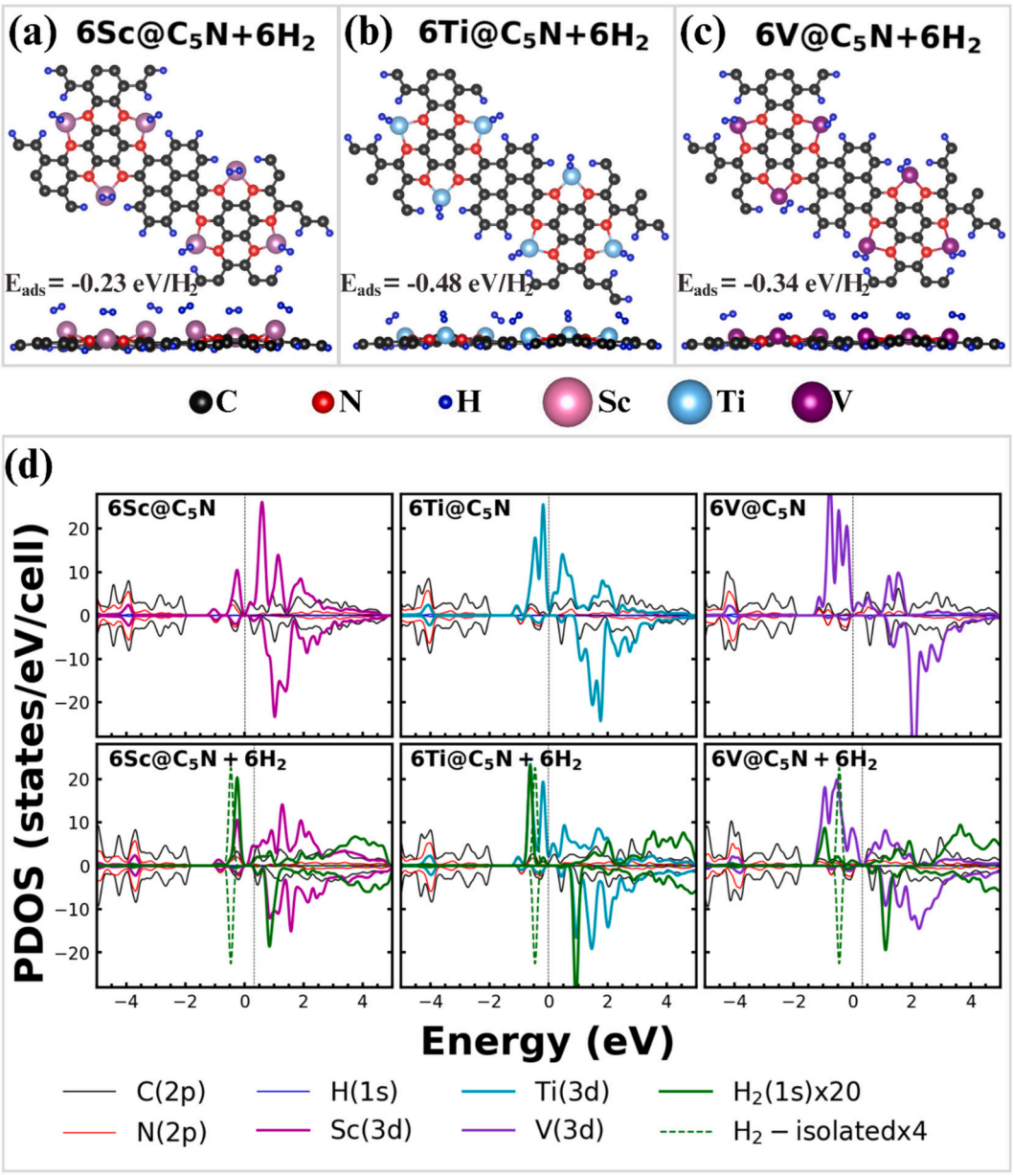

Fig. 5. Top and side views of the optimized atomic structures of (a) 6Sc@C_5N + 6H_2, (b) 6Ti@C_5N + 6H_2, and (c) 6V@C_5N + 6H_2. (d) The PDOS of 6TM@C_5N before (top) and after (bottom) 6H_2 adsorption. Here, the Fermi level is shifted to zero and shown by the black dotted line.

atoms. The optimized molecular orientations and the corresponding E_{ads} of a H_2 molecule are presented in Fig. S1. At all adsorption sites, the calculated E_{ads} are less than

-0.005 eV/molecule, indicating insufficiently weak physisorption to retain H_2 molecules at practical temperatures and pressures, resembling other 2D C_xN_y such as C_3N_4 [30] and C_2N [38]. This minimal H_2-affinity is likely attributed to the low N/C ratio with a smaller number of C—N bonds (*i.e.*, approaching the graphene or nano-porous graphene characters, which are H_2-inactive). Hence, pristine C_5N monolayer is conclusively unsuitable for H_2-storage applications.

To magnify the H_2 adsorption, surface functionalization *via* decorating selected light TMs (namely Sc, Ti, and V) with the partially filled *d*-orbitals is considered. The TMs energetically prefer to bind over C_5N at the site IX (hollow site) near N atoms with the corresponding binding energies (E_b) of Sc, Ti, and V of −4.01, −4.02, and − 3.97 eV, respectively, as shown in Fig. 1(c-h). The corresponding bond lengths are 2.09 Å (Sc—N), 2.03 Å (Ti—N), and 1.99 Å (V—N). These bond lengths are within the sum of the atomic radii for N (0.56 Å), Sc (1.84 Å), Ti (1.76 Å), and V (1.71 Å) [46], confirming strong chemical TMs-N bonds. Moreover, the diffusion barriers for the adsorbed TMs moving from their most stable positions to nearby equivalent sites were calculated using the Nudge Elastic Band (NEB) method [47]. Fig. 2 shows the possible diffusion paths and corresponding barriers of Sc, Ti, and V. Path 1 represents the diffusion across the C—N hexagon, whereas path 2 denotes the diffusion across the carbon hexagon. The diffusion barriers for path 1 of Sc, Ti, and V are 1.85, 1.69, and 2.16 eV, respectively. Meanwhile, the diffusion barriers for path 2 of Sc, Ti, and V are 1.46, 1.55, and 1.96 eV, respectively. These diffusion barriers are relatively lower than those reported for C_3N_4 and C_2N [48,49], likely due to the reduced number of C—N bonds in C_5N, which strongly interact with TMs. Nevertheless, the diffusion barriers in C_5N remain sufficiently high to stabilize single-atom catalysts (SACs) or even dual-atom catalysts (DACs). Generally, TMs tend to cluster due to their high cohesive energies. However, the clustering of TMs on H_2-storage materials is undesirable because the heavy atomic masses consequently lower the storage capacity. The combinations of magnitudes of the binding energies and diffusion barriers of

Table 1
Adsorption energies (E_{ads}) and average bond length of H_2 ($R_{H\text{-}H}$) in single and double sides, and storage capacities of gravimetric and volumetric for 6TM@C_5N (TM = Sc, Ti, and V) in theory (at 0 K).

System	E_{ads} (eV/H_2)		$R_{H\text{-}H}$ (Å)		Theoretical Storage Capacities (at 0.0 K)	
	Single side	Double sides	Single side	Double sides	Gravimetric (wt%)	Volumetric (kg/Å^3)
6Sc@C_5N						
$6H_2$ + 6Sc@C_5N	−0.2316		0.840		1.017	0.008
$12H_2$ + 6Sc@C_5N	−0.2578	−0.2029	0.812	0.798	2.014	0.016
$24H_2$ + 6Sc@C_5N	−0.2525	−0.2449	0.788	0.777	3.950	0.032
$36H_2$ + 6Sc@C_5N	−0.2131	−0.2051	0.785	0.778	5.810	0.049
Average	−0.2387	−0.2176	0.806	0.784		
6Ti@C_5N						
$6H_2$ + 6Ti@C_5N	−0.4769		0.811	–	1.003	0.008
$12H_2$ + 6Ti@C_5N	−0.2667	−0.3109	0.787	0.792	1.986	0.016
$24H_2$ + 6Ti@C_5N	−0.2704	−0.1987	0.796	0.767	3.894	0.032
$36H_2$ + 6Ti@C_5N	−0.2995	−0.1585	0.803	0.766	5.730	0.049
Average	−0.3283	−0.2227	0.799	0.775		
6 V@C_5N						
$6H_2$ + 6 V@C_5N	−0.3452		0.800		0.988	0.008
$12H_2$ + 6 V@C_5N	−0.1743	−0.2104	0.772	0.772	1.956	0.016
$24H_2$ + 6 V@C_5N	−0.1334	−0.1690	0.764	0.786	3.837	0.032
$36H_2$ + 6 V@C_5N	−0.1844	−0.1424	0.783	0.773	5.647	0.049
Average	−0.2093	−0.1739	0.778	0.777		

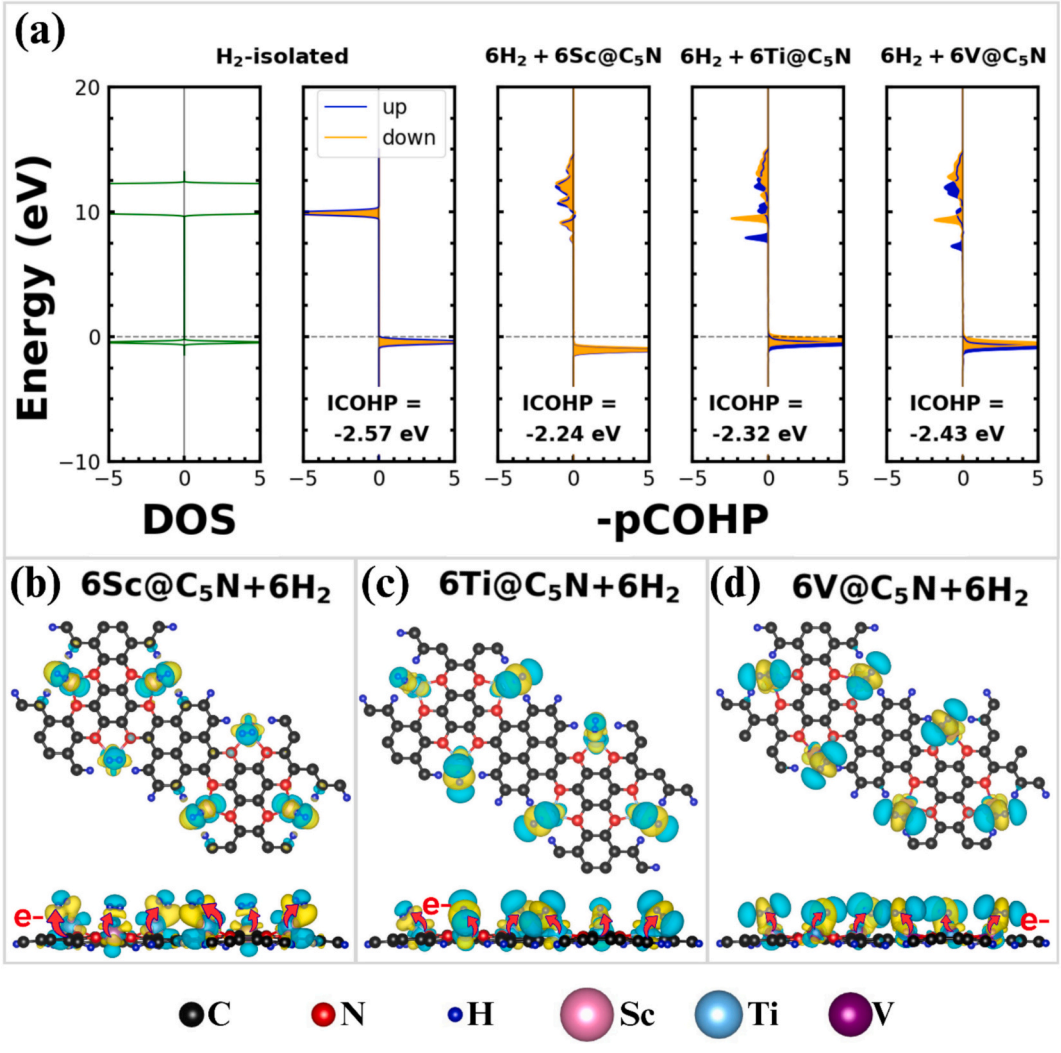

Fig. 6. (a) DOS and COHP analysis of isolated-H_2 molecule and $6H_2$ molecules adsorbed on 6TM@C_5N. Top and side views of charge density difference (CDD) of $6H_2$-adsorbed (b) 6Sc@C_5N, (c) 6Ti@C_5N, and (d) 6V@C_5N. The isosurface here is set to 0.002 eV/Å^3, and the yellow (cyan) represents charge accumulation (depletion). (For interpretation of the references to colour in this figure legend, the reader is referred to the web version of this article.)

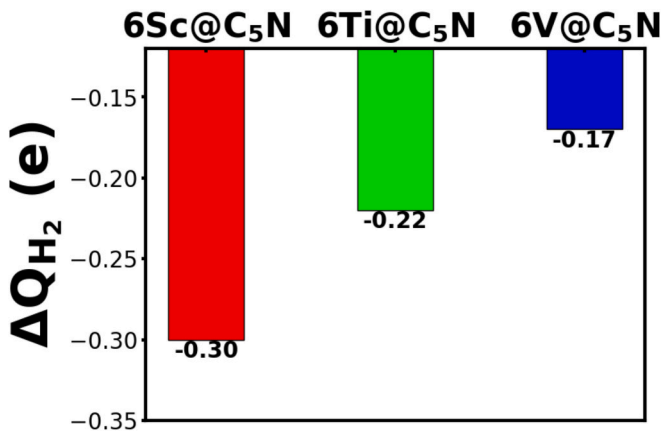

Fig. 7. Bader charge analysis of the H_2 molecules adsorbed on 6TM@C_5N.

Sc@, Ti@, and V@C_5N are 5.86, 5.98, and 6.03 eV, respectively. These values exceed the magnitudes of their corresponding bulk cohesive energies of Sc (3.9 eV), Ti (4.85 eV), and V (5.31 eV), thus energetically preventing the aggregation.

We subsequently investigated the maximum number of TMs that can be adsorbed over C_5N. This material can accommodate a maximum of six TMs per unit cell, corresponding to a high 6.25 at.% doping concentration, which is the experimentally achievable doping concentration [50]. The optimized structures of 6TMs@C_5N are shown in Fig. 3(a-c). The average E_b values of Sc, Ti, and V are −4.13, −4.23, and − 4.03 eV/dopant, respectively, being close to the binding energies of single dopants. Thus, the self-interactions among the dopants are clearly minimal at doping concentration 6.25 at.%. The average bond lengths of Sc—N, Ti—N and V—N in TMs-decorated C_5N are 2.06, 2.00, and 1.98 Å, respectively. These short bond distances incorporated by the immense binding energies manifest that the TMs are anchored on C_5N by chemical bonds which can be further elucidated by the analysis of the electronic properties.

3.2. Electronic properties of TMs-doped C_5N

Fig. 3(d) shows the spin polarized projected density of states (PDOS). Pristine C_5N is characterized as a semiconductor with an energy band gap of 1.93 eV based on the PBE level of theory. The valence band edge is dominated by the C-2*p* orbitals which are highly delocalized because of the delocalization of C π-electrons [40]. On the other hand, the conduction band edge is shared by both C-2*p* and N-2*p* orbitals. Notably, the introduction of TMs to C_5N transforms TMs@C_5N to be spin-polarized. There are states right below the Fermi energy, which are derived from the hybridization of TM-3*d* states with N-2*p* orbitals (*i.e.*, the formation of TMs-N bonds). This hybridization is attributed to the charge transfer from 3*d* states which is accepted by the high-lying N-2*p* states of C_5N. The Fermi energies of TMs@C_5N are accordingly upshifted to the conduction band. Additionally, the PDOS of the 3*d* states of independent TMs are comparatively included. There are remarkable variations of the 3*d* states before and after being decorated on C_5N, consistently indicating the formation of Sc—N, Ti—N, and V—N chemical bonds. The TMs-to-C_5N charge transfer mechanism is well-supported by the Bader charge analysis [51] and the work functions (ϕ) as shown in Fig. 4(a-b). Fundamentally, the work function (ϕ) represents the minimum energy required to remove an electron from the Fermi level to the vacuum level and is expressed as

$$\phi = V_{vac} - E_F,$$

where V_{vac} is vacuum potential and E_F is the Fermi level. The Fermi energy of C_5N shifts upward under *n*-type doping and downward under *p*-type doping. In other words, the variation in the Fermi level probed by means of the work function directly reflects the direction of charge transfer between C_5N and the adsorbed TM atom and later the H_2 adsorption on TMs@C_5N. Thus, the work function is a useful tool for quantifying the hydrogen storage capacity of materials. The findings indicate that each Sc, Ti, and V donates 1.31*e*, 1.06*e*, and 0.97*e* to C_5N upon decoration, respectively. C_5N becomes *n*-type doped after adsorbing TMs to decrease its work function. Consequently, the TM dopants get polarized to be highly affinitive to adsorbing H_2 molecules.

3.3. Hydrogen storage on TMs@C_5N

The H_2 adsorption process of TMs@C_5N was performed in a stepwise manner as shown in Fig. 5(a-c). First, a single H_2 was introduced on each TM dopant and the resulting structures were fully optimized. The number of H_2 was increased gradually and the corresponding E_{ads}were calculated until the systems reached saturation. Here, the maximum number of adsorbed H_2 molecules (*i.e.*, saturation) is defined by the E_{ads} value, which is at least −0.15 eV/molecule to ensure the H_2-storage. We found that each dopant could adsorb a maximum of 6H_2 molecules, that is, a maximum of 36H_2 on each 6TMs@C_5N system as depicted in Fig. S2-S4. The resultant gravimetric capacities of 6Sc@C_5N, 6Ti@C_5N, and 6 V@C_5N are 5.81, 5.73, and 5.65 wt%, respectively, surpassing the 2025 DOE target value of 5.50 wt%. Meanwhile, Table 1 compiles obtained numbers for 6TMs@C_5N, including the E_{ads}, average bond length of H_2 ($R_{H\text{-}H}$), gravimetric capacity, and theoretical volumetric capacity at 0.0 K. The average E_{ads} values of single (double) site adsorption are −0.24 (−0.22), −0.33 (−0.22), and − 0.21 (−0.17) eV/H_2 for 6Sc@C_5N, 6Ti@C_5N, and 6V@C_5N, respectively. We observe fluctuations in the E_{ads} because of substantial rearrangements of the decorated TM atoms during successive H_2 adsorption, as illustrated in Fig. S2-S4. Notably, the values of $R_{H\text{-}H}$ indicate elongation from 0.750 Å in an isolated H_2 molecule to 0.840 Å, signifying the typical Kubas-type interaction [36,52] which can be further elucidated by the analysis of PDOS, Crystal Orbital Hamilton Population (COHP) [53], and the charge density difference (CDD).

The Kubas-type interaction defines a unique form of H_2 molecules coordinating to a transition metal (TM) center, where the H—H bond remains undissociated but weakened. This peculiar bond originates from σ-donation from the H_2 bonding orbital to an unfilled metal *d*-orbital. Afterwards, there is π-back donation from a filled metal *d*-orbital to the H_2 σ^* (anti-bonding) orbital. Fig. 5(d) shows the PDOS of 6Sc@C_5N,

Table 2
Total of Bader charges analysis: Charge donor (+), and Charge acceptor (−).

Charge ΔQ	6TM-decorated C_5N (e)			$6H_2$ adsorbed on 6TM@C_5N (e)		
	6Sc@C_5N	6Ti@C_5N	6 V@C_5N	6Sc@C_5N	6Ti@C_5N	6 V@C_5N
C	−3.079	−1.586	−1.627	−2.688	−3.162	−3.007
N	−2.327	−2.348	−2.157	−1.716	−2.269	−1.594
H	−2.454	−2.404	−2.060	−2.735	−1.486	−2.028
Sc	7.860	0	0	8.921	0	0
Ti	0	6.338	0	0	8.207	0
V	0	0	5.845	0	0	7.638
H_2	0	0	0	−1.781	−1.290	−1.009

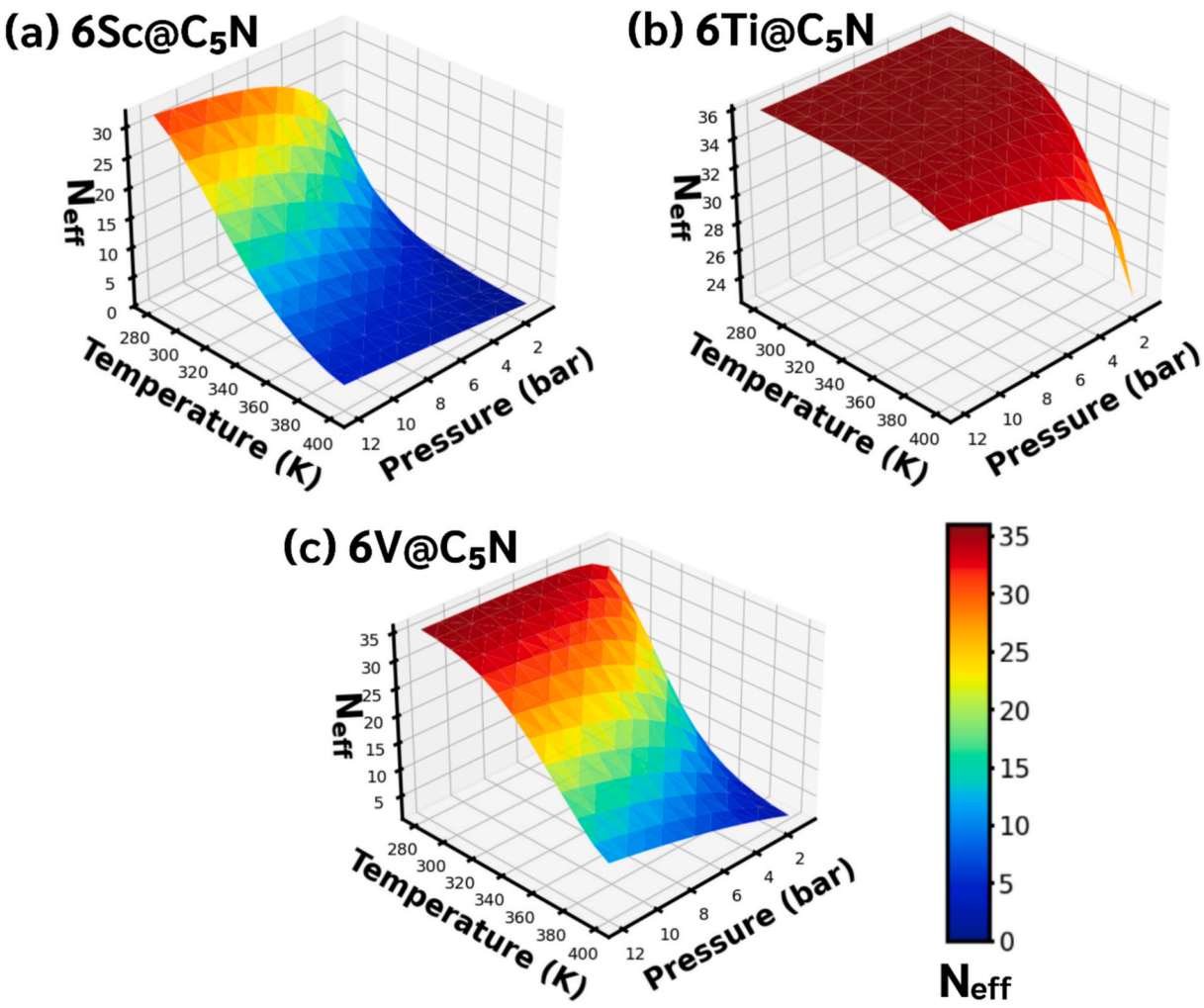

Fig. 8. Effective number of H_2 molecules (N_{eff}) adsorbed on (a) 6Sc@C_5N, (b) 6Ti@C_5N, and (c) 6V@C_5N as a function of pressures and temperatures.

Table 3
Average number of hydrogen (N_{eff}) and ratio of gravimetric capacities.

Pressure	System	Temperature				Ratio of gravimetric capacity
		298 K		355 K		
		N_{eff}	Gravimetric capacity (wt%)	N_{eff}	Gravimetric capacity (wt%)	
5 bar	**6Sc@C_5N**	27.67	4.526	4.540	0.772	82.9 %
	6Ti@C_5N	35.99	5.728	35.26	5.619	1.90 %
	6 V@C_5N	35.22	5.532	14.85	2.410	56.4 %
12 bar	**6Sc@C_5N**	31.99	5.197	9.250	1.560	70.0 %
	6Ti@C_5N	35.99	5.728	35.68	5.682	0.80 %
	6 V@C_5N	35.63	5.593	22.66	3.631	35.8 %

6Ti@C_5N, and 6V@C_5N before and after being adsorbed by H_2 molecules. There are negligible variations in C-2*p* and N-2*p* states after H_2 adsorption because of the weak interaction of C and N atoms with a H_2 molecule. On the other hand, the σ^* anti-bonding state of a free H_2 molecule becomes distinctively broadened after being adsorbed on 6TMs@C_5N, implying the charge-transfer process. This specifically coincides with the notable alteration of 3*d*-states of TMs in 6TMs@C_5N. We further elaborate on the Kubas-type interaction by analyzing COHP. Fig. 6(a) presents the COHP of H-1*s* states of an independent H_2 molecule and the adsorbed H_2 molecule on TMs-decorated C_5N. The COHP of a free H_2 molecule consists of two peaks derived from the bonding and anti-bonding states. On the other hand, the COHP of the adsorbed H_2 molecule exhibits the remarkable feature. The σ^* bonding state of the H_2 molecule is greatly perturbed, clearly indicating the reverse charge donation from the 3*d* states of TMs to the H_2 σ^* anti-bonding state. This results in the weakened interaction as supported by the less negative values of the average integrated COHP (ICOHP), *i.e.*, −2.24, −2.32, and − 2.43 eV/bond of the adsorbed H_2 molecule on $6H_2$ + 6Sc@C_5N, $6H_2$ + 6Ti@C_5N, and $6H_2$ + 6 V@C_5N, respectively, as compared with −2.57 eV/bond of an isolated H_2 molecule. Additionally, we provide insight into the electron transfer mechanism between H_2 molecules and 6TM@C_5N by calculating the CDD as shown in fig. 6(b-d). The H_2 molecule exhibits electron accumulation (yellow regions), suggesting charge transfer from the TMs to the σ^* bonding orbital of H_2. In addition, Bader charge analysis in H_2 adsorption denoted that H_2 molecules gain 0.30*e*, 0.22*e*, and 0.17*e* from Sc, Ti, and V, respectively, as shown in

Fig. 7 as Table 2.

3.4. Thermodynamic analysis for H_2 storage at practical pressure and temperature and desorption

We further investigate the H_2-storage at practical ranges of temperature and pressures, which establish the specific limits for hydrogen storage systems in light-duty vehicles following the DOE target [54]. The delivery temperature must range from −40 °C to 85 °C (233–355 K), while the storage system should deliver hydrogen at a pressure between 5 bar and 12 bar [54]. Fig. 8(a-c) show the effective number of H_2 molecules (N_{eff}) adsorbed on 6Sc@C_5N, 6Ti@C_5N, and 6V@C_5N systems as a function of temperatures and pressures according to eqs. (5)–(7). The N_{eff} values at the delivery conditions for light-duty vehicles are used to calculate the practical gravimetric capacity as compiled in Table 3. In particular, our findings manifest that the adsorption of H_2 molecules can occur within the DOE pressure range at ambient temperature (298.0 K). At 5.0 bar, the gravimetric capacities of 6Sc@C_5N, 6Ti@C_5N, and 6V@C_5N at room temperature are 4.526, 5.728, and 5.532 wt%. Meanwhile, the storage capacities are enhanced when increasing the pressure to 10.0 bar. The gravimetric capacities of 6Sc@C_5N, 6Ti@C_5N, and 6V@C_5N at room temperature are 5.197, 5.728, and 5.593 wt%, respectively. Apparently, only the storage capacities of 6Ti@C_5N, and 6V@C_5N at practical conditions are satisfactory according to the target value of DOE. For comparison, the theoretical hydrogen storage capacities of some TM-decorated C_xN_y materials at 0.0 K and 0.0 bar have been reported as 6.80 wt% for Ti-decorated C_2N [38], 8.55 wt% for Sc-decorated C_3N_4 [49], 8.55 wt% for Y-decorated C_3N_4 [55], and 6.11 wt% for Ti-decorated graphene [56].

Subsequently, we investigate the storage capacities at the elevated temperatures. Here, the ratio of gravimetric capacities between room temperature and the maximum delivery temperature is used to quantify the capability to release H_2 molecules. Notably, the ratios of 6Sc@C_5N and 6V@C_5N at 5.0 bar are 82.9 % and 56.4 %, respectively, indicating the ability to release H_2 molecules. At higher pressure of 10.0 bar, the ability to liberate H_2 molecules is relatively suppressed. The ratios of 6Sc@C_5N and 6V@C_5N are 70.0 % and 35.8 %, respectively. Our findings thus indicate that the 6Sc@C_5N and 6V@C_5N exhibit excellent reversibility, making them suitable for H_2 storage in light-duty vehicles. Note that, for 6Ti@C_5N, only a small ratio of H_2 molecules is released when the temperature increases, indicating that higher temperatures are required for efficient desorption.

Overall, considering the storage capacities at practical rages of operational pressures and temperatures and desorption temperatures, our findings indicate that 6Sc@C_5N and 6V@C_5N are suitable for efficient H_2 storage. Specifically, 6Sc@C_5N is the most promising one for light-duty vehicles because of its high H_2 molecules release rate under desired conditions. Thus, we further assess the thermal stability of this system at 400.0 K using AIMD for 5.0 ps according to the Nose-Hoover thermostat control. As shown in Fig. S5, 6Sc@C_5N is thermally stable because of the minimal fluctuations in the total energy (0.08 %) and Sc—N bond length (1.09 %).

4. Conclusion

Using various theoretical approaches including, DFT, thermodynamics, and AIMD, this work reports the H_2 storage paradigm in a light solid-state nanoporous material, *i.e.*, organic penta-carbon nitride (C_5N) decorated with light transition metals (TMs). We show that Sc, Ti, and V are favorably decorated in C_5N without aggregation because of the immense binding energies and diffusion barriers which exceed the cohesive energies of the TMs. Quantitatively, Sc, Ti, and V@C_5N attract H_2 molecules *via* the Kubas-type interaction with the storage capacities of 5.81, 5.73, and 5.65 wt%, respectively, which exceed the 5.50 wt% requirement set by the DOE. Specifically, Sc@C_5N and V@C_5N show the potentials in storing H_2 at room temperatures and low pressures with excellent desorption at practically low temperatures. Hence, transition metal decorated C_5N conclusively offer the promising functionality in H_2 storage.

CRediT authorship contribution statement

Pawitnus Kerdsombut: Writing – review & editing, Writing – original draft, Investigation, Formal analysis, Data curation, Conceptualization. **Pathipat Latthiwan:** Investigation, Formal analysis, Data curation. **Niphat Thatsami:** Visualization, Investigation, Formal analysis, Data curation. **Pakpoom Reunchan:** Validation, Funding acquisition, Conceptualization. **Adisak Boonchun:** Validation, Funding acquisition, Conceptualization. **Tanveer Hussain:** Writing – original draft, Software, Formal analysis, Conceptualization. **Supree Pinitsoontorn:** Validation, Funding acquisition, Conceptualization. **Thanayut Kaewmaraya:** Writing – review & editing, Writing – original draft, Project administration, Methodology, Investigation, Funding acquisition, Formal analysis, Conceptualization.

Declaration of competing interest

The authors declare that they have no known competing financial interests or personal relationship that could have appeared to influence the work reported in this paper.

Acknowledgements

PK would like to express my sincere gratitude to the research capability enhancement program through student scholarship, Faculty of Science, Khon Kaen University, is gratefully acknowledged for their support. This research has received funding support from the NSRF *via* the Program Management Unit for Human Resources & Institutional Development, Research, and Innovation [grant number B39G670019]). Moreover, this work is also financially supported by the fundamental fund of Khon Kaen University. The high-performance computing facility for this project was provided by Thai Supercomputing (ThaiSc) facility.

Appendix A. Supplementary data

Supplementary data to this article can be found online at https://doi.org/10.1016/j.est.2025.119608.

Data availability

Data will be made available on request.

References

[1] A.I. Osman, M. Nasr, A.S. Eltaweil, M. Hosny, M. Farghali, A.S. Al-Fatesh, D. W. Rooney, E.M. Abd El-Monaem, Advances in hydrogen storage materials: Harnessing innovative technology, from machine learning to computational chemistry, for energy storage solutions, Int. J. Hydrog. Energy 67 (2024) 1270–1294, https://doi.org/10.1016/J.IJHYDENE.2024.03.223.

[2] A. Irham, M.F. Roslan, K.P. Jern, M.A. Hannan, T.M.I. Mahlia, Hydrogen energy storage integrated grid: A bibliometric analysis for sustainable energy production, Int. J. Hydrog. Energy 63 (2024) 1044–1087, https://doi.org/10.1016/J.IJHYDENE.2024.03.235.

[3] Y. Kojima, Hydrogen storage materials for hydrogen and energy carriers, Int. J. Hydrog. Energy 44 (2019) 18179–18192, https://doi.org/10.1016/J.IJHYDENE.2019.05.119.

[4] P. Wojnarowski, D. Janiga, Enhanced system for hydrogen storage and conversion into green methanol in a geothermal environment, Int. J. Hydrog. Energy 52 (2024) 834–844, https://doi.org/10.1016/J.IJHYDENE.2023.10.133.

[5] J. Shen, Q. Zhang, S. Tian, X. Li, J. Liu, J. Tian, The role of hydrogen in iron and steel production: Development trends, decarbonization potentials, and economic impacts, Int. J. Hydrog. Energy 92 (2024) 1409–1422, https://doi.org/10.1016/J.IJHYDENE.2024.10.368.

[6] L. Esposito, M. van der Wiel, C. Acar, Hydrogen storage solutions for residential heating: A thermodynamic and economic analysis with scale-up potential, Int. J. Hydrog. Energy 79 (2024) 579–593, https://doi.org/10.1016/J.IJHYDENE.2024.06.279.

[7] P. Lykas, N. Georgousis, E. Bellos, C. Tzivanidis, A comprehensive review of solar-driven multigeneration systems with hydrogen production, Int. J. Hydrog. Energy 48 (2023), https://doi.org/10.1016/j.ijhydene.2022.09.226.

[8] L. Schlapbach, A. Züttel, Hydrogen-storage materials for mobile applications, Nature 414 (2001), https://doi.org/10.1038/35104634.

[9] J. Graetz, New approaches to hydrogen storage, Chem. Soc. Rev. 38 (2009), https://doi.org/10.1039/b718842k.

[10] W. Fang, C. Ding, L. Chen, W. Zhou, J. Wang, K. Huang, R. Zhu, J. Wu, B. Liu, Q. Fang, X. Wang, J. Wang, Review of hydrogen storage technologies and the crucial role of environmentally friendly carriers, Energy Fuel 38 (2024) 13539–13564, https://doi.org/10.1021/acs.energyfuels.4c01781.

[11] J. Ren, N.M. Musyoka, H.W. Langmi, M. Mathe, S. Liao, Current research trends and perspectives on materials-based hydrogen storage solutions: A critical review, Int. J. Hydrog. Energy 42 (2017), https://doi.org/10.1016/j.ijhydene.2016.11.195.

[12] A.P.I. Popoola, S.A. Raji, Metal Alloys for Hydrogen Storage Applications: Solid-State Hydrogen Storage in Metal-Based Materials, Elsevier, 2025.

[13] M.V. Lototskyy, M.W. Davids, I. Tolj, Y.V. Klochko, B.S. Sekhar, S. Chidziva, F. Smith, D. Swanepoel, B.G. Pollet, Metal hydride systems for hydrogen storage and supply for stationary and automotive low temperature PEM fuel cell power modules, Int. J. Hydrog. Energy (2015), https://doi.org/10.1016/j.ijhydene.2015.01.095.

[14] J. Zhang, S. Yan, H. Qu, Recent progress in magnesium hydride modified through catalysis and nanoconfinement, Int. J. Hydrog. Energy 43 (2018), https://doi.org/10.1016/j.ijhydene.2017.11.135.

[15] A. Demirbas, Storage and transportation opportunities of hydrogen, energy sources, part B: Economics, Plan. Policy 2 (2007), https://doi.org/10.1080/15567240600629419.

[16] C. Crisafulli, S. Scir, M. Salanitri, R. Zito, S. Calamia, Hydrogen production through NaBH4 hydrolysis over supported Ru catalysts: An insight on the effect of the support and the ruthenium precursor, Int. J. Hydrog. Energy 36 (2011), https://doi.org/10.1016/j.ijhydene.2010.12.089.

[17] H.W. Langmi, J. Ren, B. North, M. Mathe, D. Bessarabov, Hydrogen storage in metal-organic frameworks: A review, Electrochim. Acta 128 (2014), https://doi.org/10.1016/j.electacta.2013.10.190.

[18] E. Klontzas, E. Tylianakis, G.E. Froudakis, Designing 3D COFs with enhanced hydrogen storage capacity, Nano Lett. 10 (2010), https://doi.org/10.1021/nl903068a.

[19] A.G. Klechikov, G. Mercier, P. Merino, S. Blanco, C. Merino, A.V. Talyzin, Hydrogen storage in bulk graphene-related materials, Microporous Mesoporous Mater. 210 (2015), https://doi.org/10.1016/j.micromeso.2015.02.017.

[20] M. Hirscher, M. Becher, Hydrogen storage in carbon nanotubes, J. Nanosci. Nanotechnol. 3 (2003), https://doi.org/10.1166/jnn.2003.172.

[21] B. Viswanathan, Carbon nanomaterials as one of the options for hydrogen storage, Eng. Mater. Des. (2024), https://doi.org/10.1007/978-981-99-9935-4_15.

[22] R. Kumar, P.S. Kumar, A. Khan, A.M. Asiri, H. Dzudzevic-Cancar, Carbon-based nanomaterials for hydrogen production and storage applications, Nanomaterials for Hydrogen Storage Applications (2020), https://doi.org/10.1016/B978-0-12-819476-8.00011-6.

[23] L. Elias, S.M.A. Shibli, Surface-modified carbon nanotubes for hydrogen storage, ACS Symp. Ser. (2022), https://doi.org/10.1021/bk-2022-1425.ch007.

[24] U.S. Harisankar, S.K. Menon, J.S. Babu, B. Shankar, Exploring carbon nanotubes for enhanced hydrogen storage: A review on synthesis, mechanisms, and evaluation, Korean J. Chem. Eng. (2024), https://doi.org/10.1007/s11814-024-00311-1.

[25] M. Bucuci, Ş. Ungureanu, A. Miron, A.C. Cziker, Hydrogen Storage Potential of the Graphitic Carbon Nitride, in: Proceedings of, 10th international conference on modern power systems, MPS 2023 (2023) 2023, https://doi.org/10.1109/MPS58874.2023.10187412.

[26] R. Pachaiappan, S. Rajendran, P.S. Kumar, D.V.N. Vo, T.K.A. Hoang, L. Cornejo-Ponce, Recent advances in carbon nitride-based nanomaterials for hydrogen production and storage, Int. J. Hydrog. Energy 47 (2022), https://doi.org/10.1016/j.ijhydene.2021.09.062.

[27] A. Hashmi, M.U. Farooq, I. Khan, J. Son, J. Hong, Ultra-high capacity hydrogen storage in a Li decorated two-dimensional C2N layer, J Mater Chem A Mater 5 (2017) 2821–2828, https://doi.org/10.1039/c6ta08924k.

[28] P. Gao, X. Chen, J. Li, Y. Wang, Y. Liao, S. Liao, G. Zhu, Y. Tan, F. Zhai, Computational evaluation of Al-decorated g-CN nanostructures as high-performance hydrogen-storage media, Nanomaterials 12 (2022), https://doi.org/10.3390/nano12152580.

[29] P. Gao, J. wen Li, J. Zhang, G. Wang, Computational exploration of magnesium-decorated carbon nitride (g-C3N4) monolayer as advanced energy storage materials, Int. J. Hydrog. Energy 46 (2021) 21739–21747, https://doi.org/10.1016/j.ijhydene.2021.04.049.

[30] L. Zhang, D. Ren, W. Ding, High hydrogen storage ability of a decorated g-C3N4 monolayer decorated with both Mg and Li: A density functional theory (DFT) study, Int. J. Hydrog. Energy 47 (2022) 28548–28555, https://doi.org/10.1016/j.ijhydene.2022.06.175.

[31] C. Chen, J. Xiang, L. Ye, J. Tao, X. Chen, P. Gao, C. Zhang, Enhanced physical hydrogen storage in g-C10N3 monolayer with lithium decoration: A first-principles study, Int. J. Hydrog. Energy 95 (2024) 747–754, https://doi.org/10.1016/j.ijhydene.2024.11.126.

[32] K. Raja K, T. Anusuya, V. Kumar, DFT study of hydrogen interaction with transition metal doped graphene for efficient hydrogen storage: Effect of d-orbital occupancy and Kubas interaction, Phys. Chem. Chem. Phys. 25 (2022), https://doi.org/10.1039/d2cp03794g.

[33] S. Li, Z. Xin, Y. Luo, J. Pan, G. Liao, Q. Li, Y. Sun, Z. Feng, R. Tan, Recent advances in the development of single atom catalysts for oxygen evolution reaction, Int. J. Hydrog. Energy 82 (2024) 1081–1100, https://doi.org/10.1016/J.IJHYDENE.2024.08.026.

[34] M. Zhang, X. Lu, Z. Wu, N. Sun, X. Liu, Y. Wang, L. Wang, D. Yan, Advanced development of dual-atom catalysts: From synthesis methods to versatile electrocatalytic applications, J. Power Sources 613 (2024) 234923, https://doi.org/10.1016/J.JPOWSOUR.2024.234923.

[35] G.J. Kubas, Dihydrogen complexes as prototypes for the coordination chemistry of saturated molecules, Proc. Natl. Acad. Sci. 104 (2007), https://doi.org/10.1073/pnas.0609707104.

[36] E. Klontzas, E. Tylianakis, G.E. Froudakis, On the enhancement of molecular hydrogen interactions in nanoporous solids for improved hydrogen storage, J. Phys. Chem. Lett. 2 (2011), https://doi.org/10.1021/jz2005368.

[37] C.H. Chung, J. Ihm, H. Lee, Recent progress on Kubas-type hydrogen-storage nanomaterials: From theories to experiments, J. Korean Phys. Soc. 66 (2015) 1649–1655, https://doi.org/10.3938/jkps.66.1649.

[38] P. Panigrahi, M. Desai, M.K. Talari, H. Bae, H. Lee, R. Ahuja, T. Hussain, Selective decoration of nitrogenated holey graphene (C2N) with titanium clusters for enhanced hydrogen storage application, Int. J. Hydrog. Energy 46 (2021) 7371–7380, https://doi.org/10.1016/j.ijhydene.2020.11.222.

[39] P. Panigrahi, A. Kumar, A. Karton, R. Ahuja, T. Hussain, Remarkable improvement in hydrogen storage capacities of two-dimensional carbon nitride (g-C3N4) nanosheets under selected transition metal doping, Int. J. Hydrog. Energy 45 (2020) 3035–3045, https://doi.org/10.1016/j.ijhydene.2019.11.184.

[40] J. Mahmood, E.K. Lee, H.J. Noh, I. Ahmad, J.M. Seo, Y.K. Im, J.P. Jeon, S.J. Kim, J. H. Oh, J.B. Baek, Fused aromatic network with exceptionally high carrier mobility, Adv. Mater. 33 (2021), https://doi.org/10.1002/adma.202004707.

[41] B. Mortazavi, M. Shahrokhi, F. Shojaei, T. Rabczuk, X. Zhuang, A.V. Shapeev, A first-principles and machine-learning investigation on the electronic, photocatalytic, mechanical and heat conduction properties of nanoporous C5N monolayers, Nanoscale 14 (2022), https://doi.org/10.1039/d1nr06449e.

[42] J.P. Perdew, K. Burke, M. Ernzerhof, Generalized gradient approximation made simple, Phys. Rev. Lett. 77 (1996), https://doi.org/10.1103/PhysRevLett.77.3865.

[43] S. Grimme, Density functional theory with London dispersion corrections, Wiley Interdiscip Rev Comput Mol Sci 1 (2011), https://doi.org/10.1002/wcms.30.

[44] S. Grimme, Semiempirical GGA-type density functional constructed with a long-range dispersion correction, J. Comput. Chem. 27 (2006), https://doi.org/10.1002/jcc.20495.

[45] W. Jr. Chase Malcolm, NIST-JANAF Thermochemical Tables, in: Fourth Edition, American Chemical Society; American Institute of Physics for the National Institute of Standards and Technology, Washington, DC; New York, 1998, https://doi.org/10.18434/T42S31.

[46] E. Clementi, D.L. Raimondi, W.P. Reinhardt, Atomic screening constants from SCF functions. II. Atoms with 37 to 86 electrons, J. Chem. Phys. 47 (1967), https://doi.org/10.1063/1.1712084.

[47] G. Henkelman, B.P. Uberuaga, H. Jónsson, Climbing image nudged elastic band method for finding saddle points and minimum energy paths, J. Chem. Phys. 113 (2000), https://doi.org/10.1063/1.1329672.

[48] S.L. Li, H. Yin, X. Kan, L.Y. Gan, U. Schwingenschlögl, Y. Zhao, Potential of transition metal atoms embedded in buckled monolayer g-C3N4 as single-atom catalysts, Phys. Chem. Chem. Phys. 19 (2017), https://doi.org/10.1039/c7cp05195f.

[49] B. Chakraborty, P. Mane, A. Vaidyanathan, Hydrogen storage in scandium decorated triazine based g-C3N4: Insights from DFT simulations, Int. J. Hydrog. Energy 47 (2022), https://doi.org/10.1016/j.ijhydene.2022.02.185.

[50] J. Zou, Z. Cai, Y. Lai, J. Tan, R. Zhang, S. Feng, G. Wang, J. Lin, B. Liu, H.M. Cheng, Doping concentration modulation in vanadium-doped monolayer molybdenum disulfide for synaptic transistors, ACS Nano 15 (2021), https://doi.org/10.1021/acsnano.1c00596.

[51] E. Sanville, S.D. Kenny, R. Smith, G. Henkelman, Improved grid-based algorithm for Bader charge allocation, J. Comput. Chem. 28 (2007), https://doi.org/10.1002/jcc.20575.

[52] G.J. Kubas, Dihydrogen complexes as prototypes for the coordination chemistry of saturated molecules, Proc. Natl. Acad. Sci. 104 (2007), https://doi.org/10.1073/pnas.0609707104.

[53] R. Dronskowski, P.E. Blöchl, Crystal orbital Hamilton populations (COHP). Energy-resolved visualization of chemical bonding in solids based on density-functional calculations, J. Phys. Chem. 97 (1993), https://doi.org/10.1021/j100135a014.

[54] U.S. Department of energy, DOE Technical Targets for Onboard Hydrogen Storage for Light-Duty Vehicles, Https://Www.Energy.Gov/Eere/Fuelcells/Doe-Technical-Targets-Onboard-Hydrogen-Storage-Light-Duty-Vehicles (n.d.).

[55] P. Mane, A. Vaidyanathan, B. Chakraborty, Graphitic carbon nitride (g-C3N4) decorated with yttrium as potential hydrogen storage material: Acumen from quantum simulations, Int. J. Hydrog. Energy 47 (2022), https://doi.org/10.1016/j.ijhydene.2022.04.184.

[56] S. Chu, L. Hu, X. Hu, M. Yang, J. Deng, Titanium-embedded graphene as high-capacity hydrogen-storage media, Int. J. Hydrog. Energy 36 (2011), https://doi.org/10.1016/j.ijhydene.2011.07.015.